AD-A169 871 STRESS ANALYSIS OF METALLIC ROCKET - MOTOR CASES REINFORCED WITH A VISCOE..(U) ROYAL ARMAMENT RESEARCH AND DEVELOPMENT ESTABLISHMENT FORT HA.. 1/1

UNCLASSIFIED A GROVES ET AL. MAR 86 RARDE-9/84 F/G 21/8 NL

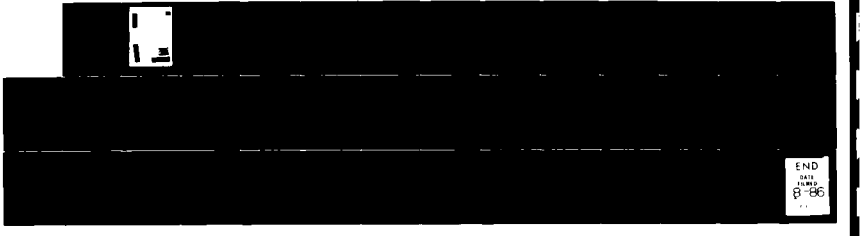

END
DATE FILMED
8-86

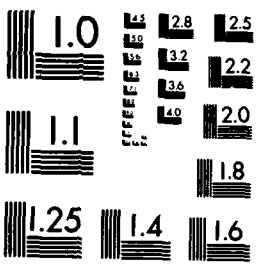

UNLIMITED

MINISTPY OF DEFFNCE

ROYAL ARMAMENT RESEARCH AND DEVELOPMENT ESTABLISHMENT

REPORT 9/84

Stress Analysis of Metallic Pocket-Motor Cases Reinforced with a Viscoelastic Fibre Overwind

A Groves
J Margetson
P Stanley*

Summary

Analytical stress solutions are presented for a metallic rocket motor case reinforced with a prestrained fibre overwind, with viscoelastic properties, under both constant and varying temperature histories. The treatment is in terms of the "reduced time" proposed by Schwarzl and Staverman, with the Williams/Landel/Ferry form of the "shift function".

The analysis is reduced to the solution of a Volterra integral equation. For a constant temperature history and using the "standard linear solid" representation of the material properties of the overwind, this equation can be solved in closed form. For varying temperature histories the equation is solved using a finite-difference technique proposed by Lee and Roger and improved by Margetson. The effects of fibre relaxation on the internal pressure required for the initiation of yield in the motor case are evaluated and discussed for a number of temperature histories and end conditions.

* Simon Engineering Laboratories, University of Manchester

CONTENTS

1 INTRODUCTION

In an effort to construct rocket-motor cases with greater specific strengths, several attempts have been made to utilise the higher strength maraging steels. This has resulted in serious quality-assurance problems, often associated with reduced ductility, and, in some instances, rocket motors have been observed to fail in a brittle manner.

With the choice of suitable constituent materials, however, a composite motor case can be constructed with a specific strength which exceeds that of any homogeneous steel design. A lightweight alloy case overwound with a high strength polyamide fibre is a particular example. Moreover, if the fibre is wound under tension a compressive stress is induced in the case, reducing the net tensile stresses developed in operation, and effectively increasing the specific strength. However, this strength-enhancement technique can create problems associated, for instance, with the dependence of the mechanical properties of the overwind on environmental conditions and sustained loading[1]. Nevertheless, the considerable possible gains in specific strength often outweigh these potential disadvantages.

A recent extensive study of the behaviour of the overwound rocket motor case[2-4] has included analyses of the initial winding process, the effect of changes in the thermal environment and the behaviour of the motor case on pressurisation. The work has been limited to linear elastic conditions; the effects of fibre relaxation, which is known to occur, on the initial stress state and subsequent yield behaviour of the motor have not been considered.

In this report procedures are developed for the stress analysis of a metallic motor case overwound with a thermorheologically simple, linear viscoelastic fibre. The Young's modulus of the fibre is assumed to be time-dependent; the Poisson's ratio and thermal expansion coefficients are assumed to be time-independent. These assumptions are valid given the temperature ranges considered in this work. The case material is assumed to be linear elastic up to yield.

The development of the viscoelastic analysis is presented and techniques for solving the resulting integral equation are discussed. The manner in which the storage temperature affects the relaxation rate is considered. Methods for predicting the yield pressure behaviour for various winding configurations and relaxation rates are presented, and typical numerical results are discussed.

2 CONSTITUTIVE EQUATIONS

2.1 Temperature-Independent Analysis

As a precursor to the temperature-dependent analysis, in which variations of mechanical properties with temperature are considered, the constitutive equations for temperature-independent behaviour are briefly discussed.

The viscoelastic constitutive law can be expressed either by the differential operator method[5] or, alternatively, by the more general representation of the

hereditary or Duhamel integral[6], in which the strain is treated as consisting of successive increments, applied over a sequence of times $0 \le t' \le t$, giving the stress as:

$$\sigma(t) = \varepsilon(t)E(0) - \int_0^t \frac{dE(t-t')}{dt'} \varepsilon(t')dt' \qquad (1)$$

In this equation $\sigma(t)$ and $\varepsilon(t)$ denote the components of stress and strain respectively at time t, and E(t) is the relaxation modulus.

The form of variation of the relaxation modulus E(t) with time is shown by the central curve in Figure 1; particular importance attaches to the short-term value E(0) (ie the "instantaneous" modulus) and the long-term asymptotic value $E(\infty)$ (ie the "equilibrium" or "rubbery" modulus).

2.2 Temperature-Dependent Analysis

2.2.1 Constant Uniform Temperature Change

In the preceding section no allowance was made for changes in the mechanical behaviour of the linear viscoelastic material arising from possible differences in the winding temperature and the subsequent temperature. For most suitable overwinding materials such effects are second order and may be neglected[7], but there may be applications in which the mechanical properties are significantly influenced by temperature changes and these effects cannot be neglected. This section deals with such applications and it is assumed that the structure experiences a constant spatially uniform temperature change subsequent to winding.

Early work by Leaderman[8] revealed that, by adjusting the time scale, it was possible to represent the temperature-dependence of several mechanical properties of a wide range of viscoelastic materials by means of a series of master curves. Such materials were later to be defined as "thermorheologically simple"[9].

The existence of this simple translational shift led Schwarzl and Staverman[9] to propose the following equivalence relationship between the relaxation modulus and temperature:

$$E(T,t) = E(T_o, \zeta) \quad , \qquad (2)$$

where $$\zeta = t/a_{T_o}(T) \quad . \qquad (3)$$

In the above equations T denotes the temperature, T_o a reference temperature, t the time elapsed from the completion of winding, and ζ the "reduced" or "shifted" time, related to the real time via the "shift function" $a_{T_o}(T)$.

Since the relaxation curve (see Fig 1) shifts to the left for a temperature increase and to the right for a temperature decrease, it follows that for T greater than T_o, $a_{T_o}(T)$ is less than unity and vice versa. It is noteworthy that both the instantaneous and equilibrium moduli are temperature-independent.

The relaxation modulus at an arbitrary temperature can thus be expressed in terms of the reference temperature behaviour using a new time scale which is dependent upon the particular temperature. Expressing the stresses and strains as functions of reduced time, the viscoelastic constitutive relationship, Equation 1 becomes

$$\sigma(\zeta) = \varepsilon(\zeta)E(0) - \int_o^{\zeta} \frac{dE(\zeta-\zeta')}{d\zeta'}\varepsilon(\zeta')d\zeta' \quad . \tag{4}$$

2.2.2 Time-Dependent Uniform Temperature Change

Since the uniform temperature considered in Section 2.2.1 was constant, a simple expression for calculating the reduced time resulted. It is now necessary to extend this analysis to deal with time-dependent temperature histories. Again spatial temperature variations are assumed to be zero; the size and thermal diffusivity of the components under consideration are such that this assumption is not unrealistic. It is also necessary to assume that the shift function $^{a}T_o(T)$ at a particular temperature is independent of the prior temperature history. Experimental evidence by Williams et al[10] suggests that such an assumption is valid.

With these assumptions it follows from Equation 3 that

$$d\zeta(t) = dt/a_{T_o}(T(t)) \quad . \tag{5}$$

Hence integrating and noting that at $t = 0$, $\zeta(t) = 0$

$$\zeta(t) = \int_o^t dt'/a_{T_o}(T(t')) \quad . \tag{6}$$

In establishing a general form of the shift function, Williams et al[10] found that the empirical relationship

$$\log_{10}[a_{T_o}(T)] = \frac{-k_1(T-T_o)}{k_2+T-T_o} \quad , \tag{7}$$

in which k_1 and k_2 are material constants, gave good results for a large range of viscoelastic materials.

3 VISCOELASTIC ANALYSIS OF THE REINFORCED MOTOR CASE

For a body subjected to a series of external loads and displacements, the stresses and strains at any point must satisfy the basic requirements of equilibrium and compatibility and must conform with the appropriate constitutive relationships. Moreover, the stresses and displacements at the boundary must comply with the applied external forces and displacements.

The gradual decease in the relaxation modulus of the fibre, $E_f(\zeta)$, will result in a time-dependent expansion of the pre-stressed motor case. If $u(\zeta)$ denotes this expansion, then from elementary thin-walled cylinder theory, the initial strains in the fibres and case are modified according to the relations

$$\varepsilon_{\theta f}^{(i,n)}(\zeta) = \varepsilon_{\theta f}^{(i,n)}(0) + \frac{u(\zeta)}{R}, \quad i=1,2,\ldots,n, \tag{8}$$

$$\varepsilon_{\theta c}^{(n)}(\zeta) = \varepsilon_{\theta c}^{(n)}(0) + \frac{u(\zeta)}{R} \quad . \tag{9}$$

In these equations $\varepsilon_{\theta f}^{(i,n)}(0)$ and $\varepsilon_{\theta c}^{(n)}(0)$ are the initial strain components for the i^{th} of n fibres and the case respectively, as given in Reference 2, and ζ is the reduced time defined by Equation 6. The quantity R denotes the mean radius of the motor case.

When the composite motor is subjected to a spatially uniform temperature change, thermal strains are induced in the fibres and case, further modifying the initial strains produced during winding. In general the coefficient of expansion of the fibres (α_f) will be less than that of the case (α_c), and hence an increase in temperature will increase the compressive stress in the case and vice versa.

From a previous thermal analysis[3], it can be shown that the strains in the i^{th} fibre layer and the case resulting from a uniform temperature change $\Delta T(\zeta)$ at reduced time ζ are given respectively by

$$\varepsilon_{\theta f \Delta T}^{(i,n)}(\zeta) = \alpha_f \Delta T(\zeta) + \frac{\delta_f(\zeta)}{R}, \quad i=1,2,\ldots,n, \tag{10}$$

and

$$\varepsilon_{\theta c \Delta T}^{(n)}(\zeta) = \alpha_c \Delta T(\zeta) + \frac{\delta_c(\zeta)}{R} \quad . \tag{11}$$

These strains consist of two components, (i) a component due to unconstrained thermal expansion and (ii) an interference component ($\delta_f(\zeta)/R$ for the fibres, $\delta_c(\zeta)/R$ for the case) resulting from the interaction of the two materials.

It follows that the total strain $\varepsilon_{\theta f TOT}^{(i,n)}(\zeta)$ for the fibres may be obtained by adding Equations 8 and 10 to give

$$\varepsilon_{\theta f TOT}^{(i,n)}(\zeta) = \varepsilon_{\theta f}^{(i,n)}(0) + \Delta\varepsilon_f(\zeta) + \alpha_f \Delta T(\zeta),\ i=1,2,\ldots,n, \tag{12}$$

where

$$\Delta\varepsilon_f(\zeta) = \frac{u(\zeta)}{R} + \frac{\delta_f(\zeta)}{R} \quad . \tag{13}$$

Similarly for the case, the total strain is obtained by adding Equations 9 and 11, giving

$$\varepsilon_{\theta c TOT}^{(n)}(\zeta) = \varepsilon_{\theta c}^{(n)}(0) + \Delta\varepsilon_c(\zeta) + \alpha_c \Delta T(\zeta) \quad , \tag{14}$$

where

$$\Delta\varepsilon_c(\zeta) = \frac{u(\zeta)}{R} + \frac{\delta_c(\zeta)}{R} \quad . \tag{15}$$

As the fibres and case are assumed to remain in contact, compatibility of radial displacements requires that $\varepsilon_{\theta f \Delta T}^{(i,n)}(\zeta)$ and $\varepsilon_{\theta c \Delta T}^{(n)}(\zeta)$ are equal. It therefore follows from Equations 10, 11, 13 and 15 that

$$\Delta\varepsilon_c(\zeta) = \Delta\varepsilon_f(\zeta) + (\alpha_f - \alpha_c)\Delta T(\zeta) \quad . \tag{16}$$

Using Equation 16 the quantity $\Delta\varepsilon_c(\zeta)$ appearing in Equation 14 can be eliminated in favour of $\Delta\varepsilon_f(\zeta)$ to give

$$\varepsilon_{\theta c TOT}^{(n)}(\zeta) = \varepsilon_{\theta c}^{(n)}(0) + \Delta\varepsilon_f(\zeta) + \alpha_f \Delta T(\zeta) \quad . \tag{17}$$

In Equation 4 the strain $\varepsilon(\zeta)$ is the mechanical strain, ie the total strain minus the free thermal strain. Making the appropriate substitution for the mechanical strain from Equation 12 into Equation 4, it follows that

$$\sigma_{\theta f}^{(i,n)}(\zeta) = E_f(0)\{\varepsilon_{\theta f}^{(i,n)}(0) + \Delta\varepsilon_f(\zeta)\} - \int_0^{\zeta} \frac{dE_f(\zeta-\zeta')}{d\zeta'}\{\varepsilon_{\theta f}^{(i,n)}(0) + \Delta\varepsilon_f(\zeta')\}d\zeta',\ i=1,2,\ldots,n, \tag{18}$$

where $\sigma_{\theta f}^{(i,n)}(\zeta)$ is the stress in the i^{th} fibre layer at reduced time ζ. Similarly, the circumferential stress in the metal case at time ζ, $\sigma_{\theta c}^{(n)}(\zeta)$, follows from Equation 17 and the linear elastic stress-strain relations in the form

$$\sigma_{\theta c}^{(n)}(\zeta) = E_c\{\varepsilon_{\theta c}^{(n)}(0)+\Delta\varepsilon_f(\zeta) + (\alpha_f-\alpha_c)\Delta T(\zeta)\} \quad . \tag{19}$$

Radial stresses are small and have been omitted from these equations.

In the absence of an internal pressure, it is an equilibrium requirement that the sum of the forces associated with these stresses (ie Equations 18 and 19) is zero[3], ie

$$\sum_{i=1}^{n} \sigma_{\theta f}^{(i,n)}(\zeta)t_f + \sigma_{\theta c}^{(n)}(\zeta)t_c = 0 \quad , \tag{20}$$

where t_c and t_f denote respectively the case thickness and the effective thickness of a single fibre layer. Substituting into Equation 20 from Equations 18 and 19 for the fibre and case stresses results in the following integral equation for the unknown quantity $\Delta\varepsilon_f(\zeta)$

$$G(0)\Delta\varepsilon_f(\zeta) - \int_0^{\zeta} \frac{dG(\zeta-\zeta')}{d\zeta'}\Delta\varepsilon_f(\zeta')d\zeta' = f(\zeta) \tag{21}$$

where

$$f(\zeta) = E_c t_c[\varepsilon_{\theta c}^{(n)}(0)\{\frac{F_f(\zeta)}{E_f(0)} -1\}$$

$$-(\alpha_f-\alpha_c)\Delta T(\zeta)] \quad ,$$

and $$G(\zeta) = nE_f(\zeta)t_f + E_c t_c. \tag{22}$$

Equation 21 is a Volterra integral equation of the second kind[5] which, for a specified $f(\zeta)$ and $G(\zeta)$, has a unique solution for $\Delta\varepsilon_f(\zeta)$.

With this solution, the change in the mechanical strain in the case $\Delta\varepsilon_c(\zeta)$ can be computed from Equation 16. The corresponding stresses then follow from Equations 18 and 19. Details of the solution procedure are given in the following section.

4 SOLUTION PROCEDURE

Solutions of equations similar in form to Equation 21 may be obtained using Laplace transforms. This solution procedure eliminates the time-dependence of the system equations in favour of the transform parameter,

thereby reducing the viscoelastic analysis to an associated elastic problem. Inversion of the resulting equations yields the solution to the original viscoelastic problem.

For elementary models, eg Maxwell and Kelvin idealisations[7], analytical inversion is often possible, but these idealised solutions are usually of limited practical interest. For many practical problems, the relaxation modulus can be represented by the Dirichlet-Prony series[11]

$$F_f(\zeta) = E_f(\infty) + \sum_{j=1}^{m} E_{fj}\, e^{-\zeta/\tau_j} \tag{23}$$

where $F_f(\infty)$ and E_{fj} denote the long term modulus and the j^{th} of m Prony coefficients respectively and τ_j is the relaxation time associated with the j^{th} Prony coefficient.

Appropriate numerical techniques (eg those proposed by Bellman et al[12]) can then be used for inverting the Laplace transforms. Using this approach for the present problem, spurious oscillations in the solution were observed, particularly at times corresponding to large relaxation rates, which could not be eliminated.

An alternative solution technique was therefore developed in which the integral appearing in Equation 21 was expressed as a sequence of analytical expressions, as originally proposed by Lee and Rogers[13] and subsequently improved by Margetson[14]. If the time interval 0 to ζ is divided into a sequence of time intervals by the time values, ζ_i, i = 1,2, ..., L, such that ζ_1, = 0 and $\zeta_L = \zeta$, and the fibre strain change $\Delta\varepsilon_f(\zeta)$ is the mean value taken over the interval, Margetson has shown that the strain change $\Delta\varepsilon_f(\zeta)$, for $\zeta = \zeta_L$, can be obtained from the equation

$$\Delta\varepsilon_f(\zeta_L) = f(\zeta_L) + \sum_{j=1}^{m} nt_f E_{fj} \{S_{j,L-1} e^{-(\zeta_L-\zeta_{L-1})/\tau_j} + \tfrac{1}{2}\Delta\varepsilon_f(\zeta_{L-1})(1-e^{-(\zeta_L-\zeta_{L-1})/\tau_j})\} / \{G(0) - \tfrac{1}{2}\sum_{j=1}^{m} nt_f F_{fj}(1-e^{-(\zeta_L-\zeta_{L-1})/\tau_j})\} \tag{24}$$

In the above equation the quantity $S_{j,L}$ denotes the recurrence vector

$$S_{j,L} = S_{j,L-1} e^{-(\zeta_L-\zeta_{L-1})/\tau_j} + \tfrac{1}{2}\{\Delta\varepsilon_f(\zeta_L) + \Delta\varepsilon_f(\zeta_{L-1})\}\{1-e^{-(\zeta_L-\zeta_{L-1})/\tau_j}\} \tag{25}$$

Once $\Delta\varepsilon_f(\zeta_L)$ has been evaluated, the stress states for the fibres and case can be evaluated. It can be shown[14] that the time-dependent fibre stress, Equation 18, is given by

$$\sigma_{\theta f}^{(i,n)}(\zeta_L) = E_f(0)\Delta\varepsilon_f(\zeta_L) + \varepsilon_{\theta f}^{(i,n)}(0)E_f(\zeta_L) - \sum_{j=1}^{m} E_{fj}S_{j,L} \quad , \quad i = 1,2,\ldots,n, \tag{26}$$

where $S_{j,L}$ is the recurrence vector defined by Equation 25. For the case, the corresponding stress component then follows from the equilibrium condition given by Equation 20.

The finite difference scheme outlined above has one notable advantage over the original technique proposed by Lee and Roger[13], in that the use of the recurrence vector dispenses with the storage of all strain values other than those obtained at the last two time intervals, thus reducing the necessary computer storage and improving numerical efficiency. It is noteworthy that the finite-difference scheme introduces no complications when the time intervals are unequal. This enables larger time intervals to be utilised in the regions of small relaxation rates.

The time-marching process is initialised by defining $\Delta\varepsilon_f(0)$, ie $\Delta\varepsilon_f(\zeta_1)$. Since u(0) must be zero, it follows from Equation 13 that $\Delta\varepsilon_f(\zeta_1)$ is equal to $\delta_f(0)/R$. This quantity is readily obtained from Reference 3.

If the thermal history contains temperature discontinuities, the foregoing procedure can be applied, provided that the strain contributions due to the discontinuities are dealt with separately.

By considering the net change in the circumferential force in the n fibre layers and case due to the k^{th} thermal discontinuity it can be shown that the step change in $\Delta\varepsilon_f(\zeta)$, at $\zeta = \zeta_k$, is given by

$$\Delta(\Delta\varepsilon_f(\zeta_k)) = \frac{(\alpha_c + \alpha_f nA(0))(\Delta(\Delta T(\zeta_k)))}{1 + nA(0)} \quad ;$$

$$A(0) = \frac{E_f(0)t_f}{E_c t_c} \quad . \tag{27}$$

In the above equation the quantities $\Delta(\Delta\varepsilon_f(\zeta_k))$ and $\Delta(\Delta T(\zeta_k))$ denote the step changes in $\Delta\varepsilon_f(\zeta)$ and $\Delta T(\zeta)$ respectively at $\zeta = \zeta_k$. Once $\Delta(\Delta\varepsilon_f(\zeta_k))$ has been calculated the value is added to the immediately preceding fibre strain change. This is then substituted into the recurrence vector, Equation 25, and the solution procedure continued.

5 YIELD INITIATION PRESSURE

The composite motor must withstand all in-flight loads without excessive distortion or failure. Although set-back forces and aeroheat effects may be significant, the predominant in-flight load will always be the firing pressure. In general, motor cases have been designed so that no plastic deformation occurs under this pressure loading. Although this design approach does not make full use of the strength reserves available in the case, and in this sense is inefficient, in this work the pressure for the onset of yield has been adopted as the basis for design.

In the preceding sections the stress and strain components for the fibres have been related through a time-dependent constitutive equation, Equation 4, in which the relaxation modulus is known to decrease with time. For loading histories extending over many decades (ie 10^{-6} h t 10^{5}) the changes in the relaxation modulus will have a pronounced effect on the stress and strain states in the motor. For very short duration loading, eg the firing pressure, which lasts typically for less than one second and rarely exceeds several minutes, relaxation effects are usually neglected. Thus, for the pressurisation analysis, the stresses and strains are related through the conventional Hookean equations. In a previous analysis [3], expressions for the elastic stress changes in the fibres and case corresponding to an applied internal pressure were derived. If the pressurisation process is regarded as an instantaneous load application, these expressions can be readily incorporated with Equations 18 and 19 to give the following expressions for the stresses in the fibres and case at ζ_p, the time of pressure application:

$$\sigma_{\theta fp}^{(i,n)}(\zeta_p) = E_f(0)\{\varepsilon_{\theta f}^{(i,n)}(0) + \Delta\varepsilon_f(\zeta_p)\}$$

$$- \int_0^{\zeta_p} \frac{dE_f(\zeta_p-\zeta')}{d\zeta'}\{\varepsilon_{\theta f}^{(i,n)}(0) \qquad , \qquad (28)$$

$$+ \Delta\varepsilon_f(\zeta')\}d\zeta'$$

$$+ \frac{p_i\, RA(0)}{t_f(1+nA(0))}\{1 - \frac{\nu_c}{2}[1-\frac{R_e^2}{R^2}]\} \qquad , \; i = 1,2,\ldots,n,$$

$$\sigma_{\theta cp}^{(n)}(\zeta_p) = E_c\{\varepsilon_{\theta c}^{(n)}(0) + \Delta\varepsilon_f(\zeta_p)$$

$$+ (\alpha_f-\alpha_c)\Delta T(\zeta_p)\} \qquad (29)$$

$$+ \frac{p_i R}{t_c(1+nA(0))}\{1 + \frac{n\nu_c A(0)}{2}[1-\frac{R_e^2}{R^2}]\} \qquad .$$

In these equations ν_c denotes Poisson's ratio of the case material, R_e is the effective throat insert radius[3] and p_i the applied internal pressure.

When the final circumferential stress (Equation 29) and, where appropriate, the axial stress are known, the pressure for the onset of yield can be evaluated using the von Mises yield criterion, the most appropriate for the materials under consideration[15].

If the radial stress is again omitted from the analysis, the mathematical form of this criterion is given by

$$(\sigma_{\theta cp}^{(n)}(\zeta_p))^2 + (\sigma_{zcp}^{(n)})^2 - \sigma_{\theta cp}^{(n)}(\zeta_p)\sigma_{zcp}^{(n)} = \sigma_y^2 \qquad (30)$$

where σ_y is the uniaxial yield stress of the case material, and $\sigma_{zcp}^{(n)}$, the axial stress component induced in the case during firing, is given by

$$\sigma_{zcp}^{(n)} = p_i \frac{(R^2 - R_e^2)}{2Rt_c} \quad . \qquad (31)$$

Substituting for the circumferential and axial stress components in Equation 30 from Equations 29 and 31, a quadratic equation for the pressure for the onset of yield in the case can be derived, in which the coefficients are functions of the winding conditions, fibre-relaxation characteristics, end conditions, temperature and dimensions. The maximum allowable firing pressure is the positive root of this quadratic.

6 NUMERICAL RESULTS

To illustrate the effects of fibre relaxation on the behaviour of the overwound motor case, a sample motor (the same as that considered in Reference 3) was analysed first with a constant uniform temperature equal to the winding temperature and then for two examples of varying temperature conditions. Motor details are given in Table 1.

6.1 Constant Temperature Conditions

Because the reference temperature may differ from the winding temperature the following analysis is presented in terms of the reduced time, given by $\zeta = t/a_{T_o}(T)$, rather than the real time t.

For the purposes of illustration the viscoelastic behaviour of the overwind will be characterised by means of the Dirichlet-Prony series[11] truncated after the first two terms.

$$E_f(\zeta) = E_f(\infty) + \{E_f(0) - E_f(\infty)\}e^{-\zeta/\tau} \quad , \qquad (32)$$

where $E_f(0)$ and $E_f(\infty)$ denote the instantaneous and long-term modulus values respectively, and τ is the characteristic time, ie the time for a modulus change of 63% of the difference between the instantaneous and long-term values. This material (the standard linear solid) displays both instantaneous and asymptotic long-term elastic behaviour, and is one of the simplest characterisations of a viscoelastic solid.

With such a material it is possible to solve Equation 21 analytically to obtain the time-dependent fibre strain $\Delta\varepsilon_f(\zeta)$. Noting that $\Delta T(\zeta)$ is zero, Equation 21 modifies to:

$$G(0)\Delta\varepsilon_f(\zeta) - \int_0^{\zeta} \frac{dG(\zeta-\zeta')}{d\zeta'}\Delta\varepsilon_f(\zeta')d\zeta' = \varepsilon_{\theta c}^{(n)}(0)E_c t_c\left[\frac{E_f(\zeta)}{E_f(0)} - 1\right] \quad . \tag{33}$$

Substituting from Equation 32 into Equation 22 and thence into Equation 33, a first-order linear differential equation in $\Delta\varepsilon_f(\zeta)$ can be derived, which, with the boundary conditions $\Delta\varepsilon_f(0) = 0$, has the solution (see Annex A).

$$\Delta\varepsilon_f(\zeta) = \Delta\varepsilon_f(\infty)\{1-e^{-\gamma\zeta/\tau}\} \quad , \tag{34}$$

where $$\Delta\varepsilon_f(\infty) = \varepsilon_{\theta c}^{(n)}(0)(\lambda-1)/(1+nA(\infty)) \quad , \tag{35}$$

$$A(\infty) = E_f(\infty)t_f/E_c t_c \quad , \tag{36}$$

and $$\lambda = E_f(\infty)/E_f(0) \quad , \tag{37}$$

$$\gamma = (1+nA(\infty))/(1+nA(0)) \quad . \tag{38}$$

Once $\Delta\varepsilon_f(\zeta)$ and, as a consequence, $\Delta\varepsilon_c(\zeta)$ (see Equation 16) have been obtained, the stresses in the viscoelastic fibres and the case resulting from an applied internal pressure can be established. For the fibres the time-independent and time-dependent stress components are evaluated by substituting Equations 32 and 34 into Equation 28. Adding the resultant expression to the pressure component (see Equation 28) gives, after some manipulation

$$\sigma_{\theta fp}^{(i,n)}(\zeta_p) = \{\varepsilon_{\theta f}^{(i,n)}(0) + \Delta\varepsilon_f(\infty)\}E_f(\zeta_p)$$

$$- \Delta\varepsilon_f(\infty)\{E_f(0)e^{-\gamma\zeta_p/\tau} +$$

$$\frac{[E_f(0)-E_f(\infty)]}{1-\gamma}[e^{-\zeta_p/\tau}-e^{-\gamma\zeta_p/\tau}]\}$$

$$+ \frac{P_i RA(0)}{t_f(1+nA(0))}\{1-\frac{\nu_c}{2}[1-\frac{R_e^2}{R^2}]\} i=1,2,..,n. \quad (39)$$

Similarly, for the case, the final stress is evaluated by substituting from Equation 35 for $\Delta\varepsilon_f(\infty)$ in Equation 34 and thence into Equation 29 to give

$$\sigma_{\theta cp}^{(n)}(\zeta_p) = F_c\varepsilon_{\theta c}^{(n)}(0)\{1 + \frac{(\lambda-1)(1-e^{-\gamma\zeta_p/\tau})}{1+nA(\infty)}\}$$

$$+ \frac{p_i R}{t_c(1+nA(0))}\{1 + \frac{n\nu_c A(0)}{2}[1-\frac{R_e^2}{R^2}]\} \quad (40)$$

For a non-zero axial stress, Equation 31 may be used to eliminate p_i from Equation 40 in favour of $\sigma_{zcp}^{(n)}$, resulting in the expression

$$\sigma_{\theta cp}^{(n)}(\zeta_p) = E_c\,\varepsilon_{\theta c}^{(n)}(0)\{1 + \frac{(\lambda-1)(1-e^{-\gamma\zeta_p/\tau})}{1+nA(\infty)}\}$$

$$+ \sigma_{zcp}^{(n)}\{\frac{1}{(1+nA(0))}[\frac{2}{(1-\frac{R_e^2}{R^2})} + \nu_c nA(0)]\} \quad (41)$$

Once the total circumferential stress in the case is known the pressure for the onset of yield can be obtained by substituting Equation 40 and, where applicable, Equation 31, into Equation 30. Previous work[3] has shown that the quantity R_e has a significant effect on the yield pressure of the overwound motor. This effect is examined in the following sections in terms of the maximum and minimum values of R_e.

6.1.1 Open-Ended Solution

When R_e approaches R, the axial stress (Equation 31) tends to zero and the circumferential stress in the case (Equation 40) becomes

$$\sigma_{\theta cp}^{(n)}(\zeta_p) = E_c \varepsilon_{\theta c}^{(n)}(0)\left[1 + \frac{(\lambda-1)(1-e^{-\gamma\zeta_p/\tau})}{1+nA(\infty)}\right] + \frac{p_i R}{t_c(1+nA(0))} \quad . \tag{42}$$

Furthermore, the yield initiation pressure, p_{iy}, becomes solely dependent on the magnitude of the circumferential stress. Hence, from Equation 42, it follows that

$$p_{iy} = \frac{(1+nA(0))t_c}{R}\left\{\sigma_y - E_c \varepsilon_{\theta c}^{(n)}(0)\left[1+\frac{(\lambda-1)(1-e^{-\gamma\zeta_p/\tau})}{1+nA(\infty)}\right]\right\} . \tag{43}$$

For the Table 1 motor the variations in yield pressure with n for several values of the non-dimensional reduced time, $\hat{\zeta}_p$ (ie ζ_p/τ), are depicted in Figure 2. It can be seen from the figure that the increase of p_{iy} with n is almost linear and that for $\hat{\zeta}_p$=4, p_{iy} becomes almost identical to the fully relaxed solution ($\hat{\zeta}_p = \infty$). Since $\varepsilon_{\theta c}^{(n)}(0)$ (see Reference 2), is directly proportional to the winding strain ε_w, p_{iy} varies linearly with ε_w.

6.1.2 Closed-Ended Solution

When the quantity R_e becomes very small, ie the motor approaches its closed-ended configuration, the axial stress (Equation 31) becomes non-zero. By substituting the two principal stress expressions (Equations 31 and 40) into the yield criterion (Equation 30) a general expression for the yield pressure is obtained. For the Table 1 motor the variations of the yield pressure with n for several values of $\hat{\zeta}_p$ are shown in Figure 3. In contrast to the open-ended solution (Fig 2) the yield pressure reaches a maximum value and then decreases as additional layers are introduced. For the instantaneous elastic solution (ie $\hat{\zeta}_p = 0$), this maximum occurs with 21 layers. For the long-term solution ($\hat{\zeta}_p = \infty$), 29 layers are required. It can be shown (see Annex B) that the maximum yield pressure is independent of the initial winding configuration and the fibre-relaxation characteristics, and is equal to $4\sigma_y t_c/R\sqrt{3}$. For the sample motor this maximum pressure value is 46 MPa.

From Figure 3 it is evident that, for the Table 1 motor, the yield pressure decreases with increasing $\hat{\zeta}_p$ for all n values less than 24 and increases with increasing $\hat{\zeta}_p$ for all n values greater than 24. These contrasting trends are further evident in Figure 4, where the yield pressure is plotted against $\hat{\zeta}_p$ for different values of λ, for the two arbitrary n values of 12 and 40. For n = 12 the yield pressure is seen to decrease with decreasing λ, whereas for n = 40 the opposite occurs. It is noteworthy that when $E_f(\infty)$ becomes zero the residual stresses in the case disappear, and the pressurisation response of the motor will depend only on the instantaneous elastic modulus of the fibres.

An insight into these effects can be obtained from Figure 5, in which the elliptical von Mises yield boundary for a bi-axial stress state is plotted; the line bB in the figure represents the instantaneous elastic solution of Equation 41. It has been shown previously[3] for elastic conditions that, when the prestrained motor is pressurised, the stress response proceeds along the line bB until the point V is reached, at which point yield occurs. The corresponding yield pressure is proportional to the $\sigma_{zcp}^{(n)}/\alpha_y$ ordinate at this point and can be evaluated using Equation 31. More generally, for viscoelastic conditions, the $\sigma_{\theta cp}^{(n)}(0)/\alpha_y$ value representing the length Ob is given by the first term on the right-hand side of Equation 41, which is time-dependent, and the slope of the line is obtained from the second term of Equation 41, which is time-independent. With relaxation, therefore, the stress response line bB moves to the right in the figure, retaining the original slope, with the changing length Ob* given by $\sigma_{\theta cp}^{(n)}(\zeta_p)/\alpha_y$. The yield intercept, V, becomes V* as indicated. It is clear that, depending upon the initial position of V in relation to the acme of the ellipse and the maximum shift of the bB line, the pressure for first yield may increase, decrease or increase to a maximum and then decrease with ζ_p.

6.2 Varying Temperature Conditions

In the previous section constant temperature conditions were assumed and it was possible to obtain stress solutions and yield pressure values in closed form.

By contrast, for varying temperature conditions the stresses are obtained numerically by solving the integral Equation 21 for $\Delta\varepsilon_f(\zeta)$ and substituting into Equation 29. In representing the stress behaviour graphically, Equation 31 is used to eliminate p_i from Equation 29 to give a simple linear relationship between $\sigma_{\theta cp}^{(n)}(\zeta_p)$ and $\sigma_{zcp}^{(n)}$ of the form

$$\sigma_{\theta cp}^{(n)}(\zeta_p) = E_c\{\varepsilon_{\theta c}^{(n)}(0)+\Delta\varepsilon_f(\zeta_p)+(\alpha_f-\alpha_c)\Delta T(\zeta_p)\}$$

$$+ \sigma_{zcp}^{(n)}\left\{\frac{1}{(1+nA(0))}\left[\frac{2}{(1-\frac{R_e^2}{R^2})} + \nu_c nA(0)\right]\right\} \quad (44)$$

For the purpose of illustration, the above equation can be represented exactly as in Figure 5. The slope of the bB line is obtained from the second term on the right-hand side of Equation 44, and is independent of both temperature and time. The intercept Ob* is given by the first term on the right-hand side of Equation 44; it will be dependent on both temperature and time and its variation will be governed by the relative magnitude of the two strain components $\Delta\varepsilon_f(\zeta_p)$ and $(\alpha_f-\alpha_c)\Delta T(\zeta_p)$.

To illustrate the effects of varying temperature conditions upon the yield pressure, the Table 1 motor has been studied, overwound with 12 and 40 fibre layers and subjected to temperture histories of the form $\Delta T(t) = a \sin \omega t$, first with $a = 50°C$ and $\omega = 2\pi$ (hours^{-1}) and then with $a = 50°C$ and $\omega = 0.2\pi$ (hours^{-1}). The motor was assumed to be closed-ended with R_e equal to zero. Five complete temperature cycles were considered for both histories. Three forms of material behaviour for the overwind have been assumed;

a. elastic,

b. viscoelastic with temperature-independent properties (see Section 2.1).

c. viscoelastic with "thermorheologically simple" properties (see Section 2.2).

Nolte and Findley[16] found that a generally varying temperature history could be satisfactorily represented by a series of time intervals over which either the temperature or the temperature rate was assumed constant. In the present work, however, only the latter will be considered. For both temperature histories each thermal cycle was approximated as illustrated in Figure 6.

6.2.1 12-Layer Configuration

For the 12-layer configuration the intersection of the bB line with the ellipse (point V, Fig 5) lies to the right of the acme of the von Mises yield ellipse. Consequently the yield pressure will decrease with decreasing case pre-stress (as indicated by the length Ob), and vice versa. Since α_f is less than α_c, it follows for the elastic conditions that the yield pressure increases with increasing temperature, the opposite occurring for a decreasing temperature. For the Table 1 motor this behaviour is illustrated in Figures 7 and 8, where the yield pressure is plotted against time for the two temperature histories considered.

When viscoelastic effects are included these trends are modified. The yield pressure may, depending on the temperature history and fibre-relaxation characteristics, increase or decrease with increasing temperature. The following features are evident in Figures 7 and 8:

a. In Figure 7, with the faster temperature cycle, the variations in p_{iy} derived from the temperature-independent analysis (curve 2) follow the temperature changes with a reduction in successive peak values due to relaxation. It is evident that the time scales of the temperature changes and the relaxation effects are such that initially the former dominates. Relaxation effects are seen to be practically negligible after 5 cycles.

b. By contrast, for the thermorheologically simple analysis (curve 3, Fig 7), it is seen that after an initial increase, p_{iy} decreases with increasing temperature, indicating that relaxation effects quickly become dominant. The effect is reversed before the first temperature peak, implying near-completion of the relaxation process.

c. For the slower temperature cycle (Fig 8), it is clear that relaxation effects are dominant over the first quarter-cycle for the temperature-independent analysis (curve 2), since p_{iy} decreases with increasing temperature. (This is in contrast with curve 2, Figure 7 - see a. above.) There are no further relaxation effects after the first half-cycle.

d. Apart from the absence of the initial increase in p_{iy}, there is little difference in the prediction derived from the thermorheologically simple analysis for the fast and slow temperature cycles (see curve 3, Fig 8 and curve 3, Fig 7).

6.2.2 40-Layer Configuration

In contrast with the 12-layer configuration, the bB line (Fig 5) for the 40-layer configuration intersects the von Mises yield locus to the left of the acme of the ellipse and the yield pressure will increase with decreasing $\sigma_{\theta cp}^{(n)}(\tau_p)/\sigma_y$ and vice versa. It follows therefore that the trends described in Section 6.2.1 will be reversed. This is evident in Figures 9 and 10. Additional features worth highlighting are:

a. There is a marked lack of symmetry of the variations in p_{iy} about its mean value, particularly for the elastic analysis, for both long and short period temperature variations.

b. The amplitude of the p_{iy} variations, again particularly for the elastic analysis, is considerably greater than that observed in Figures 7 and 8.

c. In Figure 10 for the slower temperature cycle, the predicted p_{iy} values from the two viscoelastic analyses are practically identical after the first temperature cycle.

7 CONCLUSIONS

1 Solution techniques and illustrative results have been presented for the stresses developed in a cylindrical metallic motor case circumferentially overwound with a prestrained viscoelastic fibre for both constant and varying temperature histories. The internal pressure required for the initiation of yield in the reinforced case has also been determined.

2 Relaxation effects may result in either an increase or a decrease in the yield initiation pressure.

3 With a constant temperature history and assuming open-ended conditions in the cylinder (ie motors with an effective nozzle radius which approaches that of the motor case) the yield initiation pressure for a particular example increases almost linearly with the number of fibre layers (n) and decreases non-linearly with time for a given n, approaching the fully relaxed conditions at times greater than about four times the characteristic time of the fibre.

4 With a constant-temperature history and closed-ended conditions in the case, the yield-initiation pressure increases to a maximum with increasing n and thereafter decreases as additional layers are introduced. There is a markedly non-linear time-dependence, which varies with n.

5 The variations in yield-initiation pressure resulting from two sinusoidally varying temperature histories have been studied for the closed-ended configuration. The effects on the yield-initiation pressure of:

a. the period of the temperature cycle

b. the material behaviour assumptions

for two distinct winding configurations have been illustrated and discussed.

8 REFERENCES

1 Howard A — Time-Dependent Behaviour of Aromatic Polymide Yarns. Unpublished MOD(PE) Report.

2 Groves A, Margetson J, Stanley P — Stress Analysis of Fibre-Peinforced Metallic Rocket Motor Cases. Unpublished MOD (PE) Report.

3 Stanley P, Margetson J, Groves A — Analytical Stress Solutions for Fibre-Reinforced Metallic Rocket Motor Cases. Int J Mech Sci, 26, 2, 1984, pp119-130.

4 Margetson J — Stress Analysis Procedures for the Design of Fibre-Reinforced Metallic Rocket-Motor Cases. Paper AIAA-83-1330. AIAA/SAF/ASME 19th Joint Propulsion Conference, Seattle, Washington, June 1983.

5 Bland D R — The Theory of Linear Viscoelasticity. Pergamon Press, Oxford, 1960.

6 Findley W N, Lai J S, Onaron K — Creep and Relaxation of Nonlinear Viscoelastic Materials. North-Holland Publishing Company. Amsterdam, 1976.

7 Ferry J D — Viscoelastic Properties of Polymers, 2nd Edn. Wiley, New York, 1970.

8 Leaderman H — Elastic and Creep Properties of Filamentous Materials and Other High Polymers. The Textile Foundation, Washington (1943).

9 Schwarzl F, Staverman J — Time-Temperature Dependence of Linear Viscoelastic Behaviour. J Appl Phys, 23, 8, 1952, pp838-843.

10 Williams M L, Landel R F, Ferry J D — The Temperature Dependence of Relaxation Mechanisms in Amorphous Polymers and other Glass-Forming Liquids. J Am Chem Soc, 77, 1955, pp3701-3707.

11 Fitzgerald J E, Hufferd W L — Handbook for the Engineering Structural Analysis of Solid Propellants. Naval Research and Naval Weapons Center Contract N00014-67-A-0325-0001, University of Utah, May 1971.

12 Bellman R, Kalaba R E, Lockett J — Numerical Inversion of the Laplace Transform. Amer Elsevier Publ Co (1966).

13 Lee E H, Roger T G — Solution of Viscoelastic Stress Analysis Problems using Measured Creep or Relaxation Functions. J Appl Mech, 30, 1963, pp127-133.

14	Margetson J	Evaluation of Time-Dependent Stresses from Strain Gauge Readings for Viscoelastic Materials. To be published.
15	Taylor G I Quinney H	The Plastic Distortion of Metals. Phil Trans R Soc (A), 230, 1931, pp323-362.
16	Nolte K G Findley W N	Approximation of Irregular Loading by Intervals of Constant Stress Rate to Predict Creep and Relaxation of Polyurethane by Three Integral Representations. Trans Soc Rheology, 18, 1, 1974, p123.

Reports quoted are not necessarily available to members of the public or to commercial organisations.

9 NOTATION

$a_{T_o}(T)$	shift function (see Equation 7)
$A(0)$	see Equation 27
$A(\infty)$	see Equation 36
$E(t)$	relaxation modulus at time t
E_c	Young's modulus of case material
$E_f(\zeta)$	relaxation modulus of fibre overwind at reduced time
E_{fj}	j^{th} Prony coefficient (see Equation 23)
$f(\zeta)$	see Equation 22
$G(\zeta)$	see Equation 22
m	number of Prony coefficients associated with Equation 23
n	number of applied fibre layers
P_i	internal pressure
R, R_e	mean and effective throat insert radius of case respectively
$S_{j,L}$	recurrence vector (see Equation 25)
t	real time
t_f, t_c	effective fibre thickness and case thickness respectively

T_o	shift function reference temperature
$\Delta T(\zeta)$	time-dependent uniform temperature change
$u(\zeta)$	time-dependent radial expansion of motor case
α_f, α_c	thermal expansion coefficients of fibre overwind and case respectively
γ	see Equation 38
$\delta_f(\zeta), \delta_c(\zeta)$	time-dependent interference displacement of fibre and case respectively (see Equations 10 and 11)
$\epsilon(t)$	time-dependent strain (see Equation 1)
$\epsilon_{\theta f}^{(i,n)}(\zeta), \epsilon_{\theta c}^{(n)}(\zeta)$	time-dependent circumferential strain components in the i^{th} fibre layer and case respectively
$\Delta\epsilon_f(\zeta), \Delta\epsilon_c(\zeta)$	time-dependent strain changes in fibre and case (see Equations 13 and 16)
ζ	reduced time (see Equation 6)
$\hat{\zeta}$	non-dimensional reduced time (ie ζ/τ)
λ	fibre modulus ratio (ie $E_f(\infty)/E_f(0)$)
$\sigma(t)$	time-dependent circumferential stress (see Equation 1)
$\sigma_{\theta f}^{(i,n)}(\zeta), \sigma_{\theta c}^{(n)}(\zeta)$	time-dependent circumferential stress components in the i^{th} fibre layer and case respectively
σ_y	case yield stress
$\sigma_{zcp}^{(n)}$	axial stress component in metallic case
τ	characteristic time of standard linear solid
τ_j	relaxation time associated with j^{th} Prony coefficient (see Equation 23)
ν_c	Poisson's ratio of metallic case
ω	angular frequency

Subscripts

p	due to pressure application
TOT	total
ΔT	associated with a uniform change in temperature

TABLE 1 Sample Composite Motor Case Data

Case Young's modulus:	E_c	≈ 72.4 GPa
Fibre relaxation moduli:	$E_f(0)$	≈ 93.1 GPa
	$E_f(\infty)$	≈ 46.5 GPa
Characteristic time of fibre:	τ	≈ 1.0hr
Poisson's ratio:	ν_c	≈ 0.3
Case yield stress:	σ_y	≈ 470.0 MPa
Wall thicknesses:	t_c	≈ 2.0mm
	t_f	≈ 0.1mm
Motor radius:	R	≈ 47.0mm
Winding strain:	ε_w	≈ 4.0×10^{-3}
Thermal expansion coefficients:	α_c	≈ 22.5×10^{-6}/°C
	α_f	≈ 3.6×10^{-6}/°C

FIG. 1

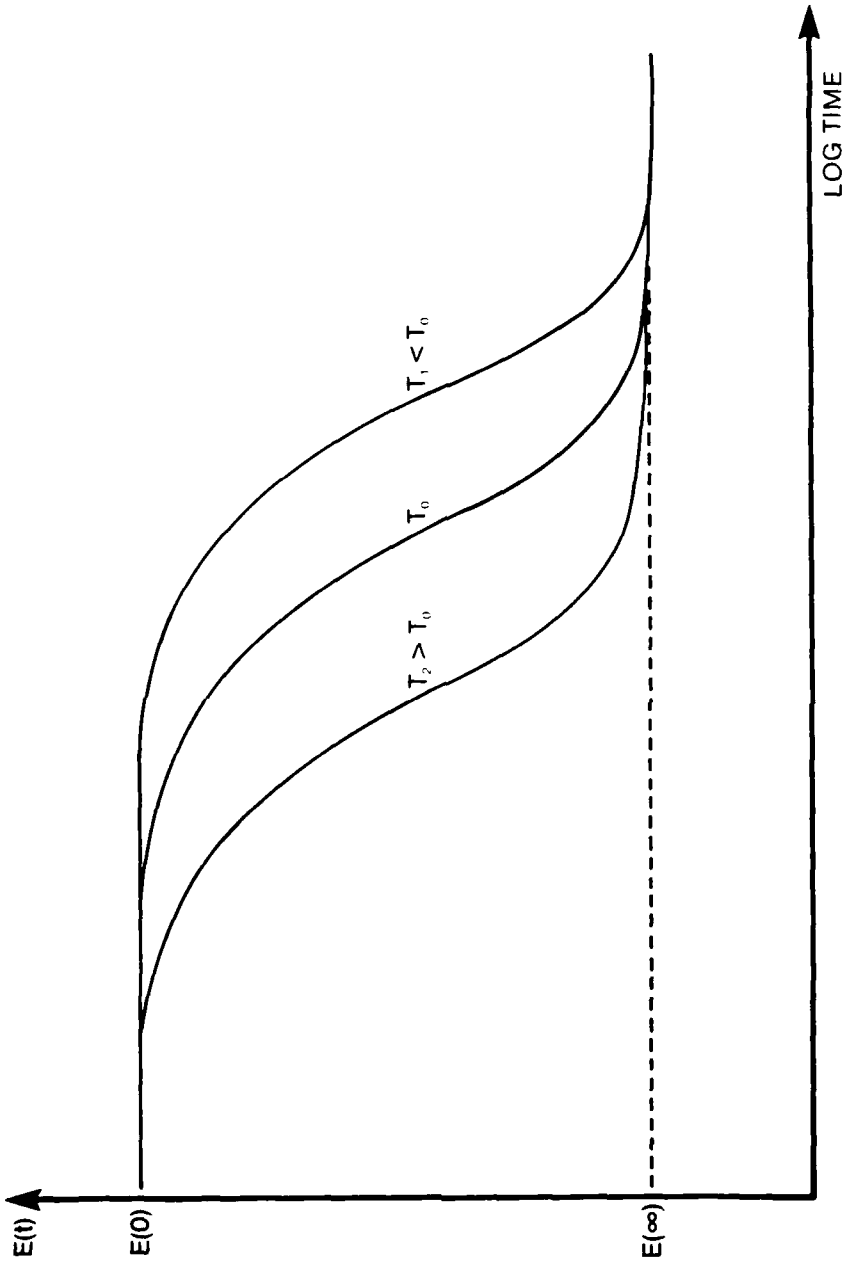

FIG. 1 TYPICAL RELAXATION MODULUS CURVES

FIG. 2

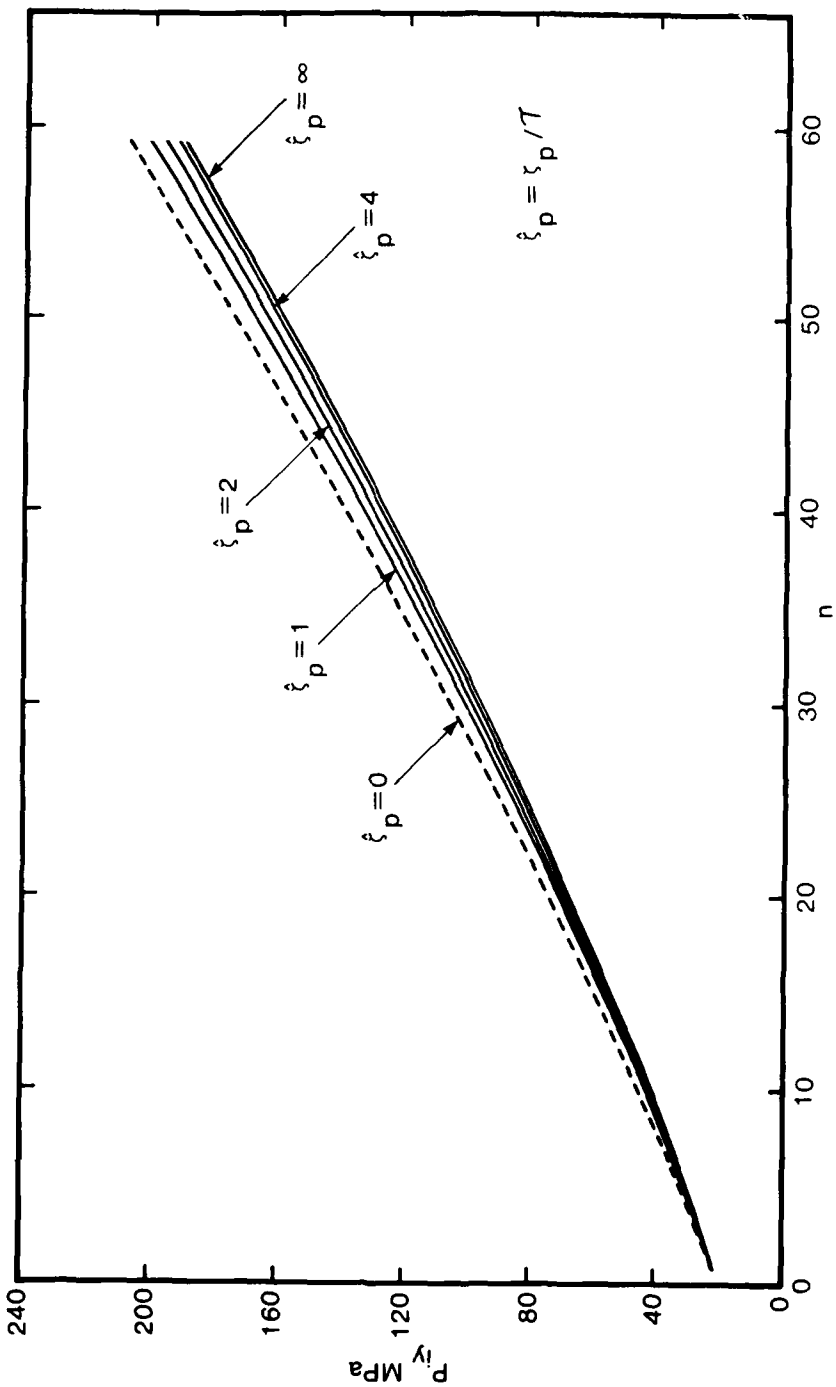

FIG. 2 P_{iy} vs n FOR VARIOUS $\hat{\xi}_p$ (OPEN-ENDED)

FIG. 3

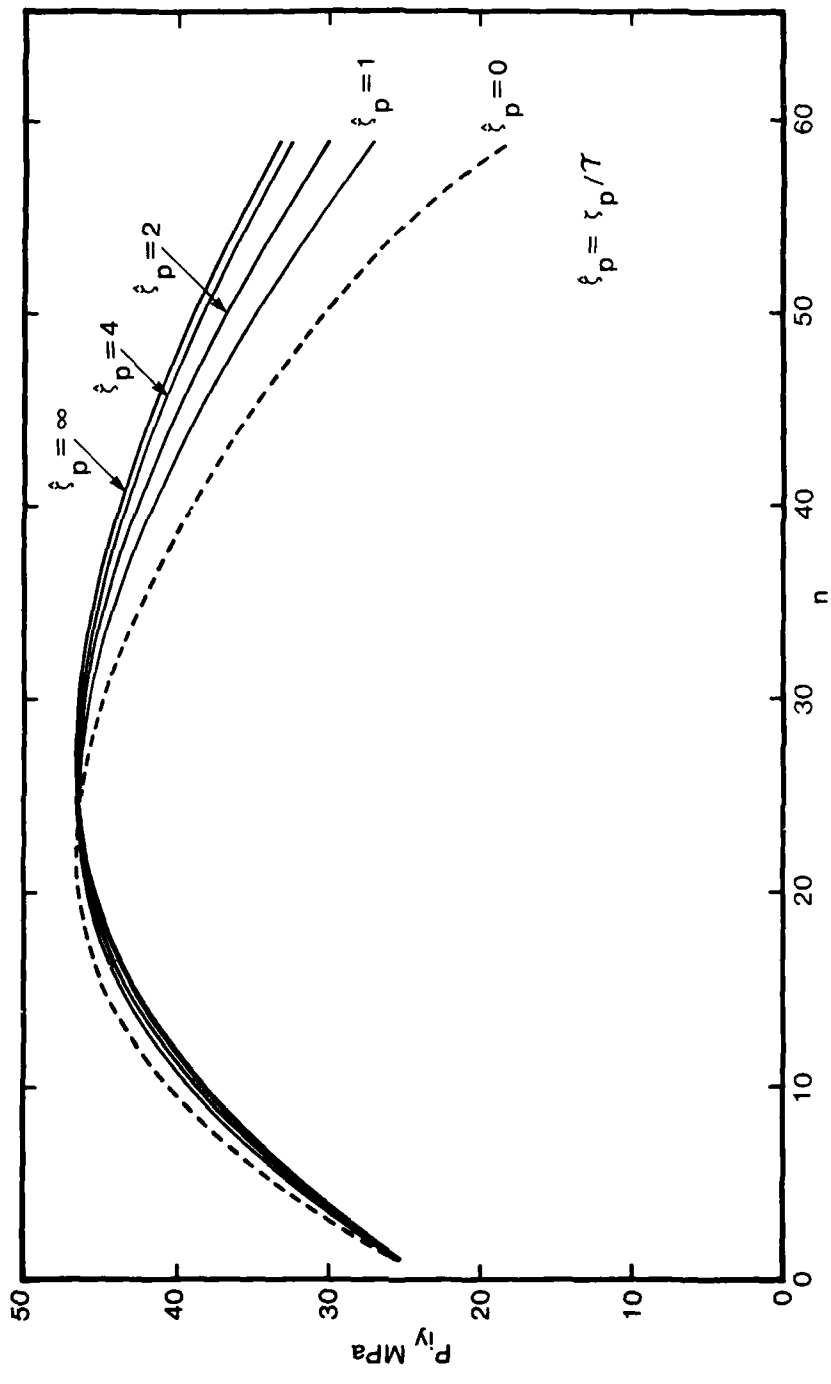

FIG. 3 P_{iy} vs n FOR VARIOUS $\hat{\zeta}_p$ (CLOSED-ENDED)

FIG. 4

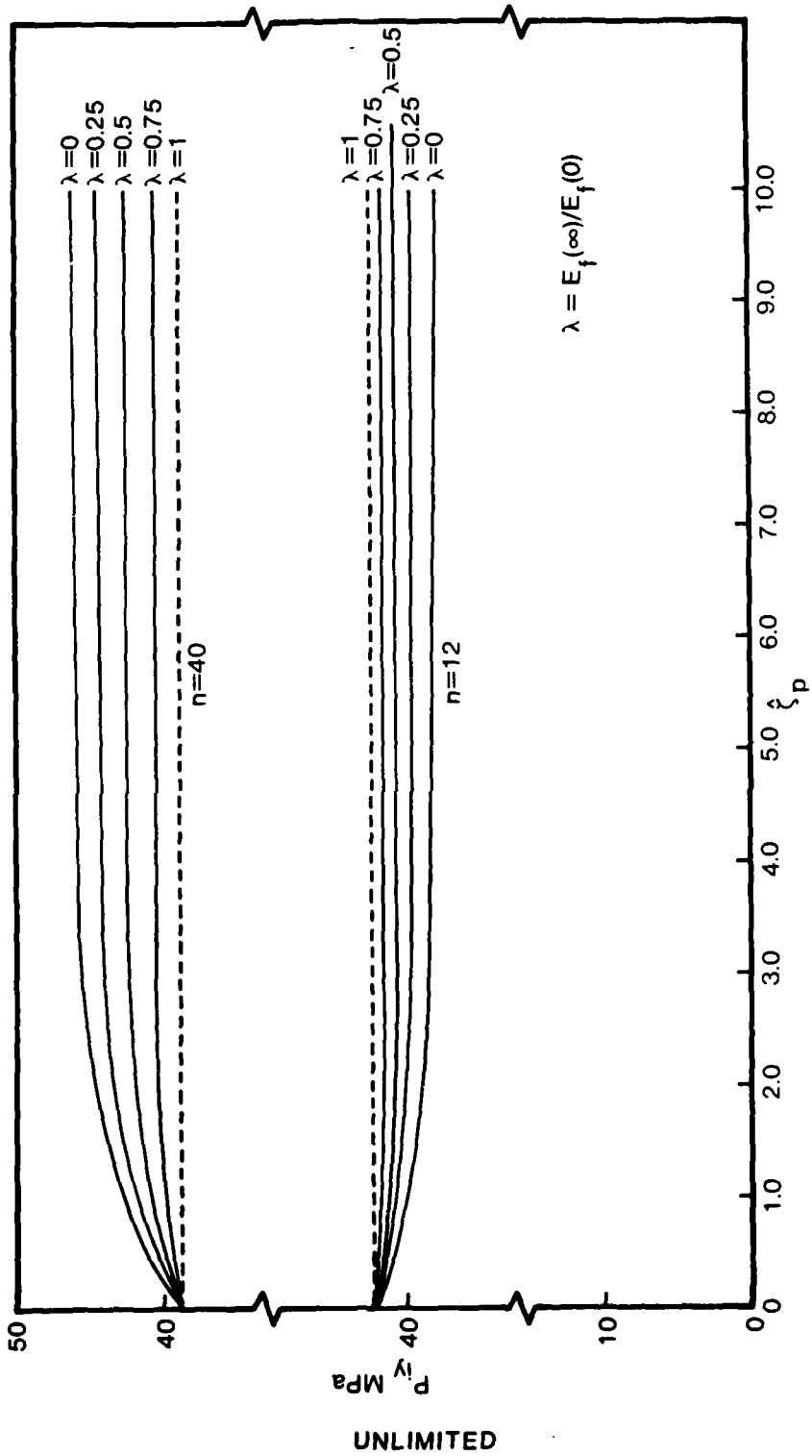

FIG. 4 P_{iy} vs ξ_p FOR n EQUAL TO 12 AND 40 FOR VARIOUS λ (CLOSED-ENDED)

FIG. 5

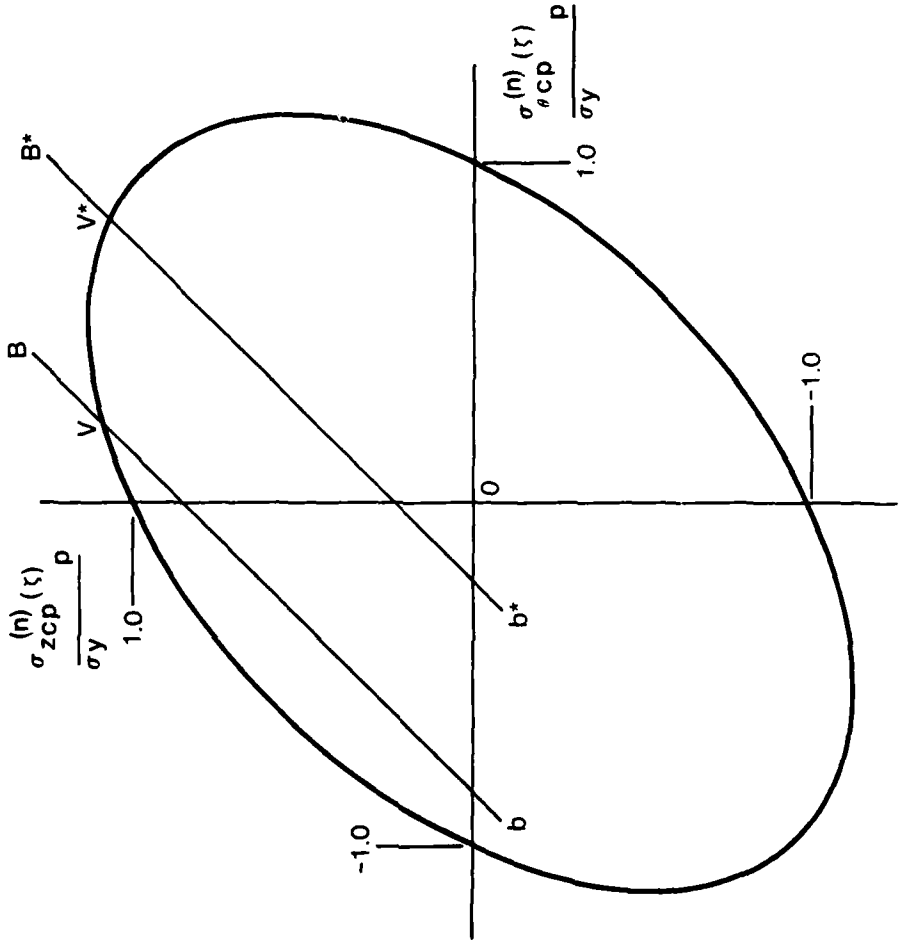

FIG. 5 von MISES YIELD LOCI

FIG. 6

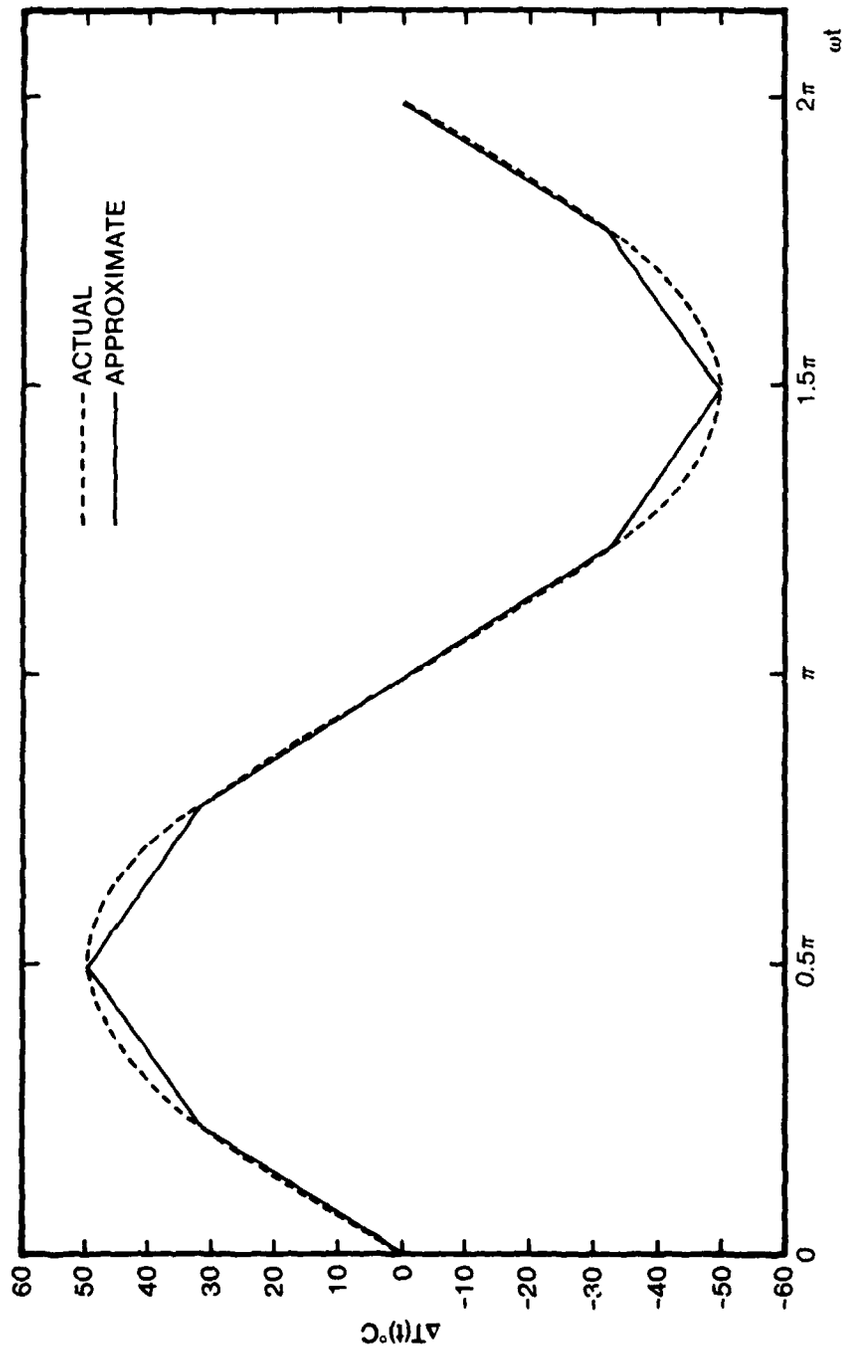

FIG. 6 $\Delta T(t)^{\circ}C$ vs ωt

FIG. 7

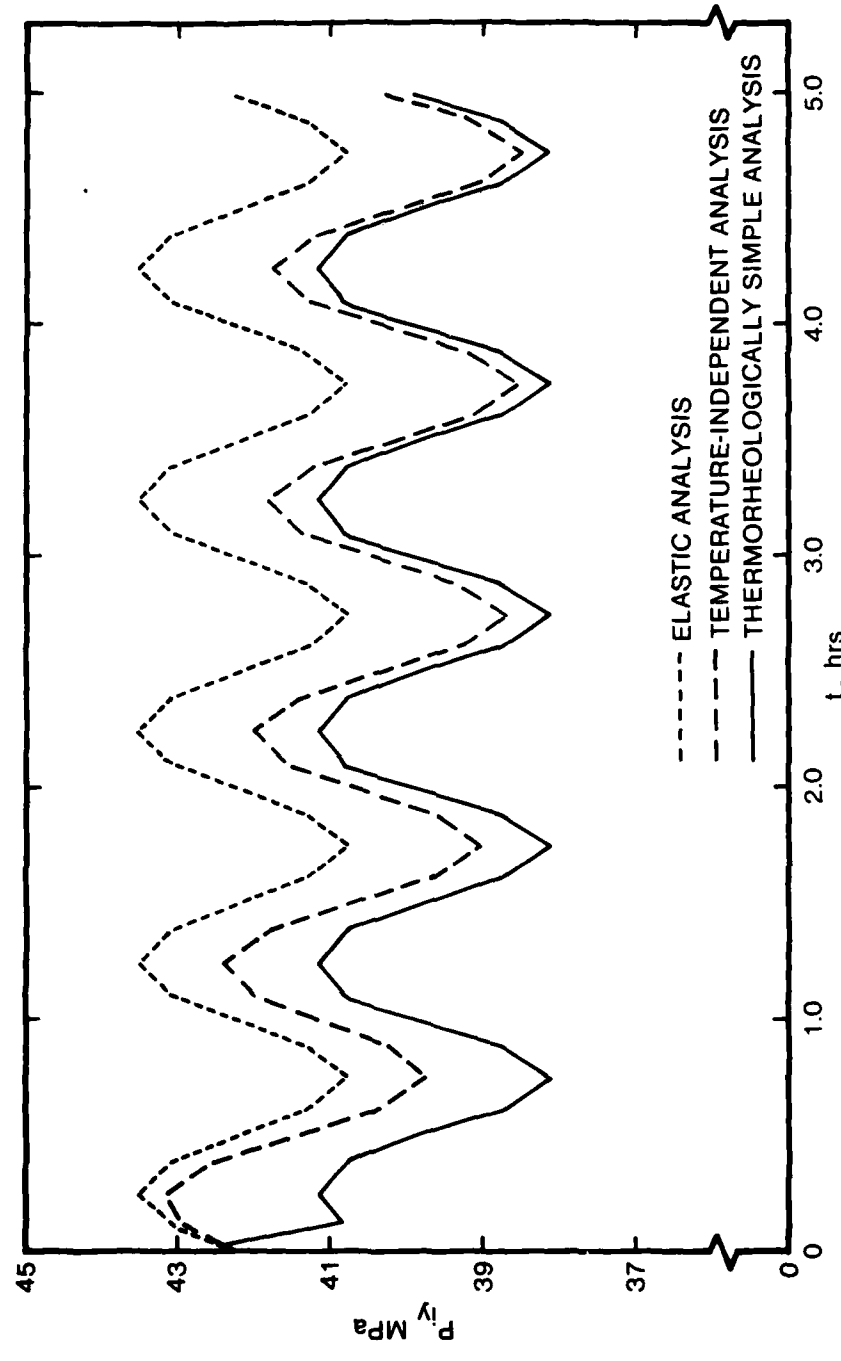

FIG. 7 P_{iy} vs t_p FOR $\Delta T(t) = 50°C \sin 2\pi t$ (n = 12 CLOSED-ENDED)

FIG. 8

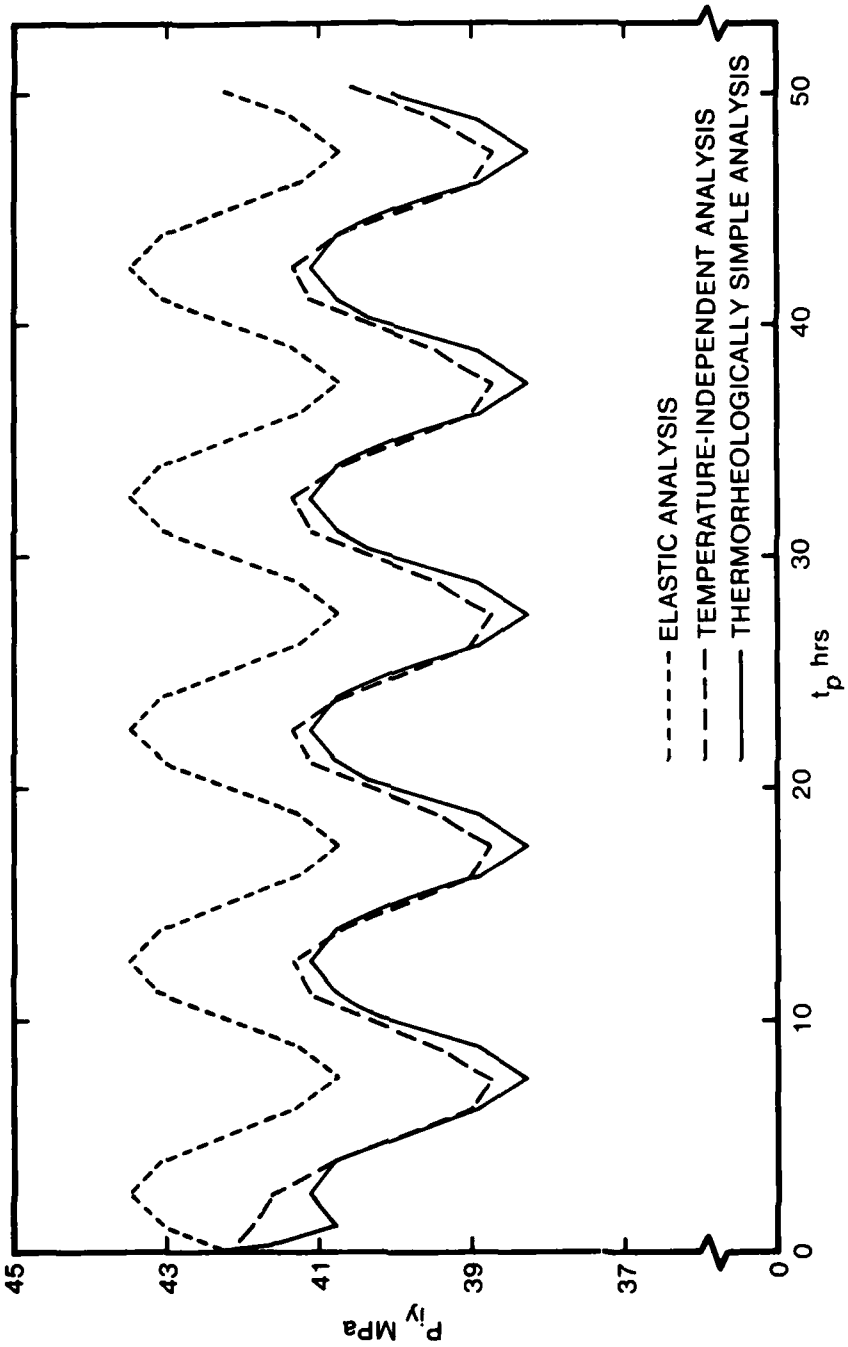

FIG. 8 P_{iy} vs t_p FOR $\Delta T(t) = 50^{\circ}C \sin 0{\cdot}2\pi t$ (n = 12 CLOSED-ENDED)

FIG. 9

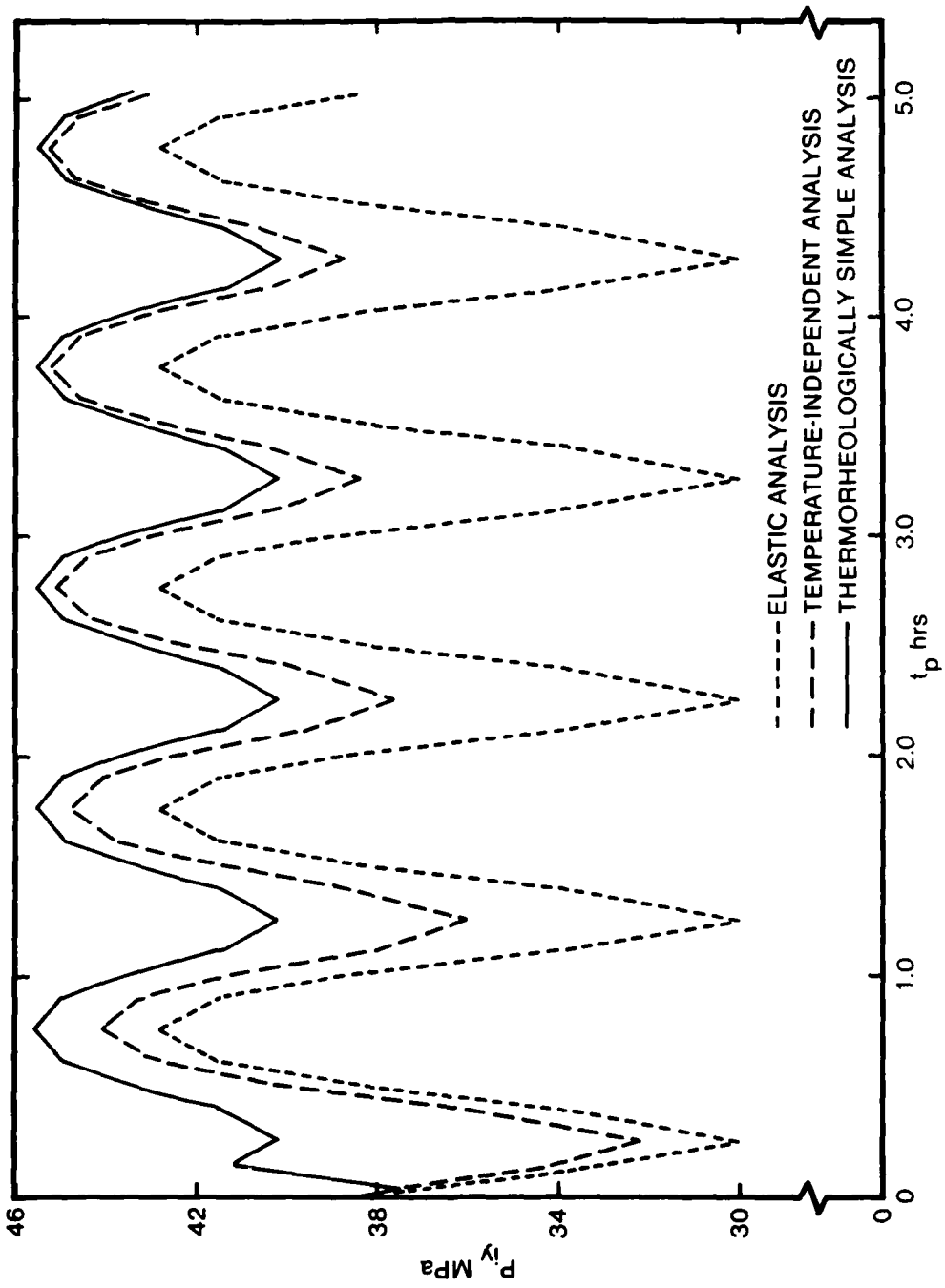

FIG. 9 P_{iy} vs t_p FOR $\Delta T(t) = 50^{\circ}C \sin 2\pi t$ (n = 40 CLOSED-ENDED)

FIG. 10

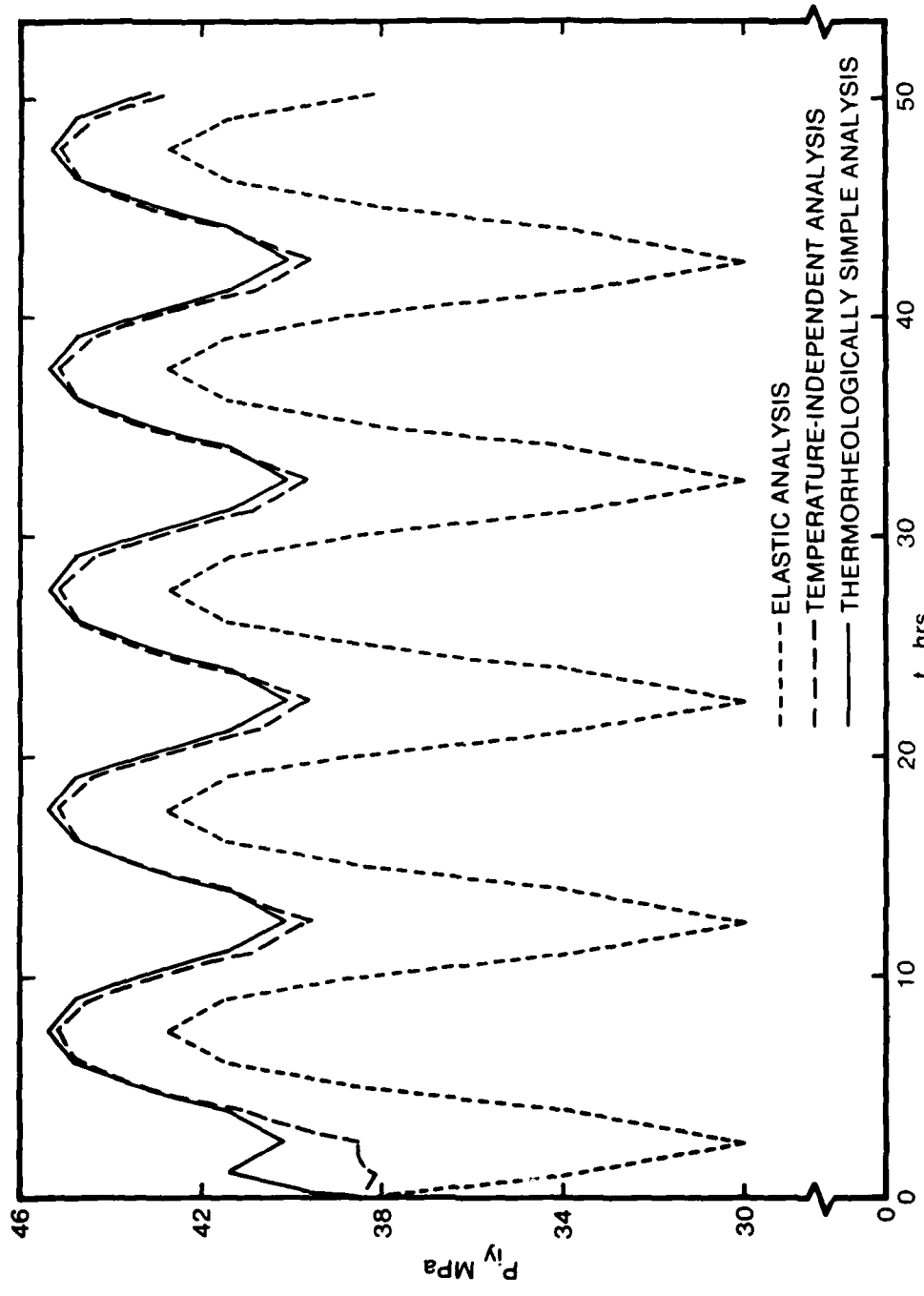

FIG. 10 P_{iy} vis t_p FOR $\Delta T(t) = 50^{\circ}C \sin 0.2\pi t$ (n = 40 CLOSED-ENDED)

ANNEX A

ANALYTICAL SOLUTION TO THE CONSTANT TEMPERATURE ANALYSIS INTEGRAL EQUATION (EQUATION 33)

In Section 6.1 the integral equation

$$G(0)\Delta\varepsilon_f(\zeta) - \int_0^{\zeta} \frac{dG(\zeta-\zeta')}{d\zeta'}\Delta\varepsilon_f(\zeta')d\zeta' = \varepsilon_{\theta c}^{(n)}(0)E_c t_c\left[\frac{E_f(\zeta)}{E_f(0)} - 1\right] \quad , \tag{A1}$$

was derived for the constant temperature analysis where, from Equation 22,

$$G(\zeta) = nE_f(\zeta)t_f + E_c t_c \quad . \tag{A2}$$

For the standard linear solid the relaxation modulus $E_f(\zeta)$ appearing in Equations A1 and A2 can be readily characterised by the truncated Dirichlet-Prony series[11], in the form

$$E_f(\zeta) = E_f(\infty) + E_1 e^{-\zeta/\tau} \quad , \tag{A3}$$

in which (see Equation 32)

$$E_1 = E_f(0)\{1-\lambda\} \quad . \tag{A4}$$

With this characterisation Equation A2 modifies to:

$$G(\zeta) = nt_f\{E_f(\infty)+E_1 e^{-\zeta/\tau}\} + E_c t_c \quad . \tag{A5}$$

Substituting from Equations A4 and A3 for $E_f(\zeta)$ in Equation A1 and noting from Equation A5 that

$$\frac{dG(\zeta-\zeta')}{d\zeta'} = G_1 e^{-(\zeta-\zeta')/\tau} \quad , \tag{A6}$$

where

$$G_1 = \frac{nt_f E_1}{\tau} \quad , \tag{A7}$$

the following modified integral equation is obtained

$$G(0)\Delta\varepsilon_f(\zeta) - G_1\int_0^{\zeta} e^{-(\zeta-\zeta')/\tau}\Delta\varepsilon_f(\zeta')d\zeta'$$

$$= \varepsilon_{\theta c}^{(n)}(0)F_c t_c \left\{\frac{F_f(\infty)+E_1 e^{-\zeta/\tau}}{F_f(0)} - 1\right\} \quad . \tag{A8}$$

Differentiating the above equation with respect to ζ gives, after some manipulation, the following first-order linear differential equation in $\Delta\varepsilon_f(\zeta)$

$$\frac{d\Delta\varepsilon_f(\zeta)}{d\zeta} + \left\{\frac{1}{\tau} - \frac{G_1}{G(0)}\right\}\Delta\varepsilon_f(\zeta) = \frac{\varepsilon_{\theta c}^{(n)}(0)(\lambda-1)}{\tau(1+nA(0))} \quad , \tag{A9}$$

which, with the boundary condition $\Delta\varepsilon_f(0)=0$, has the solution

$$\Delta\varepsilon_f(\zeta) = \Delta\varepsilon_f(\infty)(1-e^{-\gamma\zeta/\tau}) \quad , \tag{A10}$$

with

$$\Delta\varepsilon_f(\infty) = \varepsilon_{\theta c}^{(n)}(0)\frac{(\lambda-1)}{1+nA(\infty)} \quad , \tag{A11}$$

and

$$\gamma = \frac{1+nA(\infty)}{1+nA(0)} \quad . \tag{A12}$$

Once $\Delta\varepsilon_f(\zeta)$ has been obtained the corresponding strain change for the case material $\Delta\varepsilon_c(\zeta)$ then follows from Equation 16. The time-dependent fibre and case strains and stresses are then evaluated via Equations 12 and 14 and Equations 18 and 19 respectively.

ANNEX B

MAXIMUM YIELD PRESSURE ANALYSIS ISOTHERMAL CONDITIONS

If the radial stress component, which is a second-order quantity, is omitted from the von Mises yield criterion, Equation 30, the simplified expression is obtained

$$(\sigma_{\theta cp}^{(n)})^2 + (\sigma_{zcp}^{(n)})^2 - \sigma_{\theta cp}^{(n)}\sigma_{zcp}^{(n)} = \sigma_y^2 \quad , \tag{B1}$$

where the circumferential and axial stress components, $\sigma_{\theta cp}^{(n)}$ and $\sigma_{zcp}^{(n)}$ respectively, have the functional form

$$\sigma_{\theta cp}^{(n)} = \sigma_{\theta cp}^{(n)}\{p_{iy}, \zeta_p\} \quad , \tag{B2}$$

$$\sigma_{zcp}^{(n)} = \sigma_{zcp}^{(n)}\{p_{iy}\} \quad . \tag{B3}$$

These quantities are also functions of the winding conditions, moduli, geometry, etc, but for the purposes of this work they are assumed to take prescribed values.

Differentiating Equations B1, B2 and B3 with respect to ζ_p and setting $\partial p_{iy}/\partial \zeta_p$ to zero, the following relationships for the maximum yield pressure conditions can be derived

either $$\frac{\partial \sigma_{\theta cp}^{(n)}}{\partial \zeta_p} = 0 \quad , \tag{B4}$$

or $$2\sigma_{\theta cp}^{(n)} - \sigma_{zcp}^{(n)} = 0 \quad . \tag{B5}$$

Since $\sigma_{\theta cp}^{(n)}$ is a monotonically increasing function of ζ_p (see Equation 40) it follows that only the second condition, Equation B5, applies. Equation B5 can now be used to eliminate $\sigma_{\theta cp}^{(n)}$ from Equation B1 to give the simple relationship

$$\sigma_{zcp}^{(n)}\{p_{iymax}\} = \frac{2}{\sqrt{3}}\sigma_y \quad , \tag{B6}$$

where p_{iymax} denotes the maximum yield pressure. Using Equation B6, the maximum yield pressure then follows from a simple rearrangement of Equation 31, ie

$$p_{iymax} = \frac{4t_c \sigma_y R}{\sqrt{3}(R^2 - R_e^2)} \tag{B7}$$

Once p_{iymax} has been obtained, the time to the maximum yield pressure condition, ζ_{pmax}, for the standard linear solid then follows by substituting from Equation B5 for $\sigma_{\theta cp}^{(n)}$ in Equation 41, and thence from Equation B6 for $\sigma_{zcp}^{(n)}$ in the resulting equation to give, after some manipulation

$$\zeta_{p_{max}} = -\frac{\tau}{\gamma} \ln\left\{\frac{\sigma_y(2\phi-1)}{\sqrt{3}E_c \Delta\varepsilon_f(\infty)} + \frac{\varepsilon_{\theta c}^{(n)}(0)}{\Delta\varepsilon_f(\infty)} + 1\right\} \cdot \tag{B8}$$

where

$$\Delta\varepsilon_f(\infty) = \frac{\varepsilon_{\theta c}^{(n)}(0)(\lambda-1)}{1+nA(\infty)} \quad , \text{(see Equation 35)}, \tag{B9}$$

$$\phi = \frac{1}{(1+nA(0))}\left[\frac{2}{(1-\frac{R_e^2}{R^2})} + \nu_c nA(0)\right] \cdot \tag{B10}$$

Equation B8 can now be easily solved for ζ_{pmax}. Only positive values are admissible.

REPORT DOCUMENTATION PAGE

(Notes on completion overleaf)

Overall security classification of sheet .....UNLIMITED.....

(As far as possible this sheet should contain only unclassified information. If it is necessary to enter classified information, the box concerned must be marked to indicate the classification eg (R), (C), or (S)).

1. DRIC Reference (if known)	2. Originator's Reference Report 9/84	3. Agency Reference	4. Report Security Classification UNLIMITED
5. Originator's Code (if known) 7699000H	6. Originator (Corporate Author) Name and Location Ministry of Defence Royal Armament Research and Development Establishment		
5A. Sponsoring Agency's (Code (if known)	6A. Sponsoring Agency (Contract Authority) Name and Location		

7. Title Stress Analysis of Metallic Rocket-Motor Cases Reinforced with a Viscoelastic Fibre Overwind

7A. Title in Foreign Language (in the case of translation)

7B. Presented at (for conference papers). Title, place and date of conference

8. Author 1, Surname, initials	9A Author 2	9B Authors 3, 4...	10. Date	pp	ref
Groves, A.	Margetson, J.	Stanley, P.	March 1986	37	16

11. Contract number and Period	12. Project	13& 14 Other References.

15. Distribution statement

Descriptors (or keywords)		
Rocket engine cases	Fiber composites	Numerical analysis
Viscoelasticity	Reinforcing materials	Temperature
Composite materials	Polyamide resins	Applications of mathematics
	Stress analysis	Volterra equations

Abstract >Analytical stress solutions are presented for a metallic rocket motor case reinforced with a prestrained fibre overwind, with viscoelastic properties, under both constant and varying temperature histories. The treatment is in terms of the "reduced time" proposed by Schwarzl and Staverman, with the Williams/Landel/Ferry form of the "shift function". The analysis is reduced to the solution of a Volterra integral equation. For a constant temperature history and using the "standard linear solid" representation of the material properties of the overwind, this equation can be solved in closed form. For varying temperature histories the equation is solved using a finite-difference technique proposed by Lee and Roger and improved by Margetson. The effects of fibre relaxation on the internal pressure required for the initiation of yield in the motor case are evaluated and discussed for a number of temperature histories and end conditions.

END

DATE
FILMED

8-86

DTIC